Proceedings of the ASME 2010 3rd Joint US-European Fluids Engineering Summer Meeting and 8th International Conference on Nanochannels, Microchannels, and Minichannels
FEDSM-ICNMM2010
August 1-5, 2010, Montreal, Canada

FEDSM-ICNMM2010-30865

OPTIMIZATION AND ACTIVE CONTROL OF THE UNDERHOOD COOLING SYSTEM – A NUMERICAL ANALYSIS

Mahmoud Khaled
Thermofluids, Complex Flows and Energy Research Group – Laboratoire de Thermocinétique, CNRS-UMR 6607, Ecole Polytechnique
University of Nantes
Nantes, France

Fabien Harambat
Aerodynamic and Aeroacoustic Research and Development Department – PSA Peugeot Citroen
Vélizy, France

Anthony Yammine
Testing System and Turbocharging Department – Kratzer Automation
Jouy en Josas, France

Hassan Peerhossaini
Thermofluids, Complex Flows and Energy Research Group – Laboratoire de Thermocinétique, CNRS-UMR 6607, Ecole Polytechnique
University of Nantes
Nantes, France

ABSTRACT

Here numerical analysis is focused on optimizing the vehicle heat exchanger by varying the geometry in which it is integrated in the vehicle's cooling system. This analysis also elucidates how one can affect the different parameters that influence heat exchanger performance in order to optimize their functioning, in relation to the geometry in which they are integrated. The two-dimensional computational code developed permits optimizing the performance of the cooling module by positioning different heat exchangers, in both driving and stop phases of the vehicle. The ultimate aim is to develop new approaches to controlling heat exchanger positions in a real vehicle cooling system.

Keywords: Vehicle cooling system, Car thermal management, Heat exchangers, Computational code, Thermal performance, Pressure losses, Control approach, Active control.

INTRODUCTION

Heat exchangers are used in a wide variety of applications: military and aerospace, power plants, nuclear reactors, chemical and biomedical processes, the food industry, the automobile industry, robotics and metrology [1-10], to name only a few. The current trend is to reduce their volume and weight while maintaining sufficient thermal efficiencies. Several approaches to control and design are followed to optimize the heat exchangers' thermal performance [11-20]. Most previous studies concentrate on the design and geometry as well as on the fluid flow structures. However, little attention is focused on heat exchanger optimization that takes into account heat exchanger interactions with their environment.

In the present paper, numerical analysis focuses on vehicle heat exchanger optimization by taking into account the geometry of the environment in which the heat exchanger is integrated in the vehicle's cooling system as well as the vehicle underhood. This approach also elucidates how to affect the different parameters that influence heat exchanger performance in order to optimize their behavior in relation to the geometry

of the underhood environment. A two-dimensional computational code is developed using Matlab that permits optimizing the performance of the cooling system by positioning different heat exchangers in both the driving and stop phases of the vehicle. The main principle of the two-dimensional computational code is to consider the overall surface of a heat exchanger as an assembly of n×m cells, to establish thermal and aerodynamic balances at each cell and to integrate these balances throughout the overall surface.

The cooling system of a vehicle is an assembly of different heat exchangers (radiator, condenser, oil and transmission oil coolers, and charge air cooler) and one or two fans. Due to the airflow from the exterior to the underhood, the cooling system can extract a good portion of the heat in the underhood. To allow the cooling module to extract heat in difficult operating conditions, it has been pushed backward into the engine compartment. Therefore, the underhood air flow and aerothermal state are largely conditioned by the cooling system, and the performance of this system continues to present crucial aerothermal management challenges in its design as well as its interaction with other underhood components.

With respect to the air flow, heat exchangers in present cooling systems are in an 'in-rank' arrangement: each heat exchanger is positioned in a plane at a constant distance X from its nearest neighbor (Figure 1).

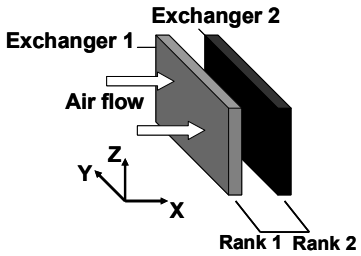

Figure 1: 'In-rank' arrangement of two vehicle heat exchangers.

In an in-rank arrangement, the heat exchangers faced uniform air flow because the air is guided by the fins and tubes of the successive heat exchangers. However, the air undergoes high pressure losses in crossing the cooling system and its temperature rises significantly as it passes through several rows of heat exchangers. This requires more fan power when the vehicle is stopped. Moreover, the cooling of heat exchangers in the second (or greater) rank and that of the bodies downstream of these heat exchangers is less efficient compared to heat exchangers directly facing cold air or components not directly downstream of the heat exchanger.
On the other hand, when integrated in environments of complex geometry (especially in actual vehicle underhoods), heat exchangers are always subjected to a nonuniform upstream flow velocity distribution that causes lower thermal power in the heat exchanger than would a uniform velocity distribution of the same flow rate. Little research has focused on the relation between nonuniformities in the upstream flow velocity and decreases in heat exchanger performance [21].

In particular, the present numerical investigation permits optimization of channels in the vehicle cooling system through optimal positioning of its different heat exchangers and optimal positioning of the system as a whole with respect to a nonuniform air velocity distribution (air inlet position).

The rest of this paper is organized as follows. The following section describes the two-dimensional code. The next section analyzes results obtained with the two-dimensional code, suggests a new control approach that permits adapting the performance of the cooling system heat exchangers to the engine thermal requirements.

NOMENCLATURE

$A(x)$	function
$B(x)$	function
C_p	specific heat of the exchanger liquid, $J.Kg^{-1}.K^{-1}$
$C_{p,air}$	air specific heat, $J.Kg^{-1}.K^{-1}$
E_r	relative difference with respect to "in-rank" configuration, %
$f(x)$	function
$g(x)$	function
h	heat exchanger overall heat transfer coefficient, $W.m^{-2}.K^{-1}$
h_{cell}	heat transfer coefficient of the heat exchanger cell, $W.m^{-2}.K^{-1}$
K	constant
m	number of heat exchanger cells by row
$\dot{m}$	heat exchanger overall liquid flow rate, $Kg.s^{-1}$
$\dot{m}_{air}$	heat exchanger overall air flow rate, $Kg.s^{-1}$
$\dot{m}_f$	heat exchanger functioning liquid flow rate, $Kg.s^{-1}$
n	number of heat exchanger cells by column
P	heat exchanger overall thermal power, kW
PL	pressure losses, Pa
$\dot{Q}_{cell}$	thermal power of heat exchanger cell, kW

ρ	heat exchanger liquid density, $Kg.m^{-3}$
S	heat exchanger overall surface, m^2
S_{cell}	heat exchanger cell surface, m^2
T	temperature, $°C$
T_a	air temperature upstream of the exchanger (ambient temperature), $°C$
$T_{a,downstream}$	air temperature downstream of the exchanger, $°C$
$T_{in,cell}$	liquid temperature at the cell inlet, $°C$
$T_{m,cell}$	mean liquid temperature through the cell, $°C$
$T_{out,cell}$	liquid temperature at the cell outlet, $°C$
u	constant
v	constant
V	air velocity, $m.s^{-1}$
V_f	heat exchanger functioning air velocity, $m.s^{-1}$
V_{cell}	heat exchanger cell air velocity, $m.s^{-1}$
x	variable
X	heat exchanger surface fraction

Computational code

The two-dimensional code used for the optimization has been developed using Matlab. It is essentially based on decomposition of the total heat exchanger matrix area into *n*×*m* cells (Figure 2).

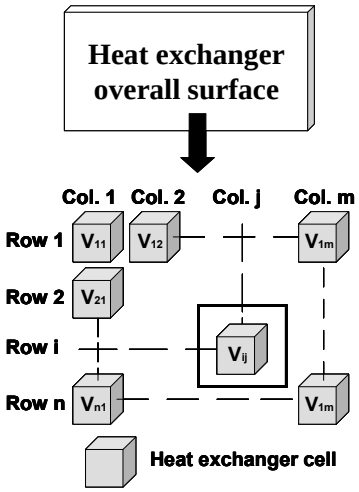

Figure 2: Heat exchanger decomposition into n×m cells.

Aerodynamic and thermal balances are applied to each elementary matrix of the heat exchanger and then integrated through the entire heat exchanger surface. Details of the aerodynamic and thermal balances are given in the following two subsections.

Thermal computation

Heat exchangers vary in their fluid flow arrangement and architecture. Among the most common are the fin and tube heat exchangers, which are composed of tubes of elliptical cross section between which are positioned several continuous and parallel fins that can be simple, crimped, shutters, or equipped with delta-wing vortex generators, etc. In many common industrial applications, particularly in the automotive industry, louvered-fin heat exchanger types are used because of their high thermal efficiency, light weight and compactness [22-26] (Figure 3).

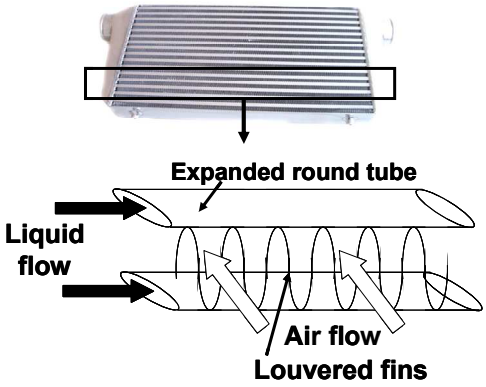

Figure 3: Schematic of louvered-fin heat exchanger.

In this type of heat exchanger, the coolant (liquid) enters at the top and is then divided among *m* vertical tubes. After moving through different vertical tubes, the liquid exits from the bottom of the heat exchanger. In this context, the following assumptions are made [27]:

- the total liquid mass flow rate in the heat exchanger is equally distributed among the different columns,
- after each passage, the liquid is perfectly mixed,
- the outlet temperature of each cell is considered equal to the inlet temperature of the following one,
- the heat transfer coefficient in each cell is equal to that of the complete heat exchanger, cooled by the same air velocity, in which the same coolant flow circulates.

The performance of a single-phase air-cooled heat exchanger is generally described by the overall heat-transfer coefficient h between the hot stream (liquid) and the cooling air as defined by:

$$P = h.S.\left[\frac{T_{in} + T_{out}}{2} - T_a\right] \quad (1)$$

where h is essentially a function of the heat-exchanger liquid flow rate and the cooling airflow rate [30]:

$$h = f(\dot{m};\dot{m}_{air}) \quad (2)$$

Assuming that the definition of the heat-exchanger overall heat transfer coefficient h in equations (1) and (2) is valid at each cell in the heat-exchanger matrix, one can then write the cell thermal power P_{cell} as:

$$P_{cell} = h_{cell}.S_{cell}(T_m - T_a)_{cell} \quad (3)$$

where T_m is the heat-exchanger hot stream mean temperature and h_{cell} is the overall heat exchanger heat transfer coefficient:

$$h_{cell} = f\left(\dot{m}_{cell};\dot{m}_{air,cell}\right) \quad (4)$$

Meanwhile, by considering the energy balance between the inlet and the exit on the hot stream side of a cell, we have:

$$P_{cell} = \dot{m}_{cell}C_p(T_{in,cell} - T_{out,cell}) \quad (5)$$

Hence, the total heat transferred between the two fluids is:

$$P = \sum_{i=1}^{N} P_{cell} = \sum_{i=1}^{N} h_{cell}.S_{cell}.(T_m - T_a)_{cell} = h.S.(T_m - T_a) \quad (6)$$

$$P = \sum_{i=1}^{N} P_{cell} = \sum_{i=1}^{N} \dot{m}_{cell}C_p(T_{in,cell} - T_{out,cell}) = \dot{m}.C_p(T_{in} - T_{out}) \quad (7)$$

Equations (6) and (7) are the basic equations for heat exchanger thermal modeling, with h always derived from experimental curves $h = f(\dot{m}_{fluid};\dot{m}_{air})$ with characteristic trends shown in Figure 4.

Experimental data from tests on the overall heat exchanger surface give discrete values of the overall transfer coefficient h of the heat exchanger (nodes shown in Figure 3): for each pair (liquid flow rate, air velocity) a single value for h is measured (note that this value is then considered the same in each cell traversed by the same (fluid flow, air velocity) pair).

In order to determine the overall heat transfer coefficient h for any pair of liquid flow rate and air velocity either between or outside the nodes, extrapolation methods described and validated in [28] and [29] of the following general form have been applied to the liquid flow rate and air velocity dependence of the overall heat-transfer coefficient:

$$h\left(\dot{m}_f;V\right) = \frac{a_{\dot{m}_f} + c_{\dot{m}_f}.V^{d_{\dot{m}_f}}}{b_{\dot{m}_f} + V^{d_{\dot{m}_f}}} \quad (8)$$

$$h\left(\dot{m};V_f\right) = \frac{a_V + c_V.V^{d_V}}{b_V + V^{d_V}} \quad (9)$$

where $\dot{m}_f$ and V_f are respectively the liquid flow rate and the air velocity of the heat exchanger and the different coefficients are calculated by iteration [21] from the different experimental data $\left(V_i;h_i\right)$ or $\left(\dot{m}_j;h_j\right)$.

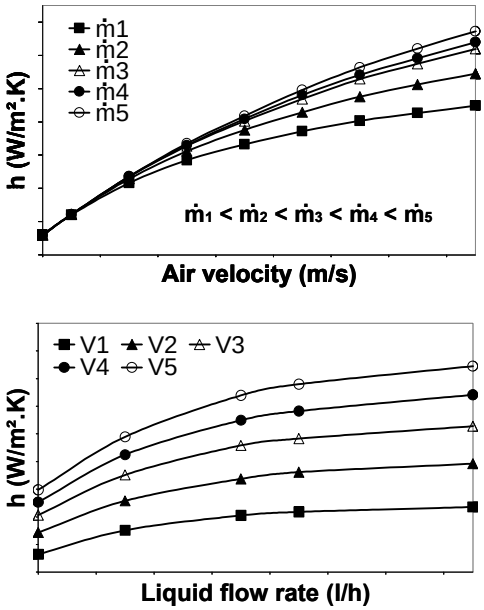

Figure 4: Characteristic experimental curves of the overall heat-transfer coefficient.

The heat flux extracted by a heat exchanger at a cell is given by the following relation:

$$\dot{Q}_{cell} = h.S_{cell}.\left(T_{m,cell} - T_a\right) = h.S_{cell}.\left(\frac{T_{in,cell} + T_{out,cell}}{2} - T_a\right) \quad (10)$$

On the other hand, by considering the thermal balance in the fluid part between the cell inlet and outlet, we can write:

$$\dot{Q}_{cell} = \dot{m}_{cell}.C_p.\left(T_{in,cell} - T_{out,cell}\right) \quad (11)$$

By combining equations (10) and (11), the temperature at the cell outlet can be obtained through the following expression:

$$T_{out,cell} = A(\dot{m}_{cell};V_{cell}).T_{in,cell} + B(\dot{m}_{cell};V_{cell}).T_a \quad (12)$$

where:

$$A(\dot{m}_{cell};V_{cell}) = \frac{2.\dot{m}_{cell}.C_p - h(\dot{m}_{cell};V_{cell}).S_{cell}}{2.\dot{m}_{cell}.C_p + h(\dot{m}_{cell};V_{cell}).S_{cell}} \quad (13)$$

$$B(\dot{m}_{cell};V_{cell}) = \frac{2.h(\dot{m}_{cell};V_{cell}).S_{cell}}{2.\dot{m}_{cell}.C_p + h(\dot{m}_{cell};V_{cell}).S_{cell}} \quad (14)$$

Also, by considering the thermal balance of the air on its passage through the heat exchanger cell, one can write:

$$T_{a,downtsream} = T_a + K.(T_{e,cell} - T_{s,cell}) \quad (15)$$

$$K = \frac{\dot{m}.C_p}{\dot{m}_{air}.C_{p,air}} \quad (16)$$

Thus, for given inlet temperature and liquid mass flow rate and for fixed air velocity distribution upstream of the heat exchanger, equations (12) to (15) are the basic equations for the present procedure for calculating the evacuated heat flux. The fluid outlet temperature and the temperature distribution of the air downstream of the heat exchanger can then be calculated. Figure 5 shows how the heat balance in a heat exchanger cell on line *i* and column *j* (Figure 5a) is introduced into a computation loop of air and fluid outlet temperatures in the entire column *j* (Figure 5b).

At each computation stage in cell *ij*, first the overall heat transfer coefficient *h(ij)* of the cell is determined by the iteration method detailed in section 4.1 (Figure 4b). The coefficient *h(ij)* is calculated for the (cooling-fluid flow rate, air velocity) pair. *V(ij)* represents the air velocity distribution corresponding to row *i* and column *j* of the matrix, over an area upstream of the heat exchanger. Then, the coefficients *A(ij)* and *B(ij)* are calculated using equations (15) and (16). From the inlet temperature of cell *ij* (which is the outlet temperature of cell (*i-1, j*)), the air temperature upstream of the heat exchanger cell and the two coefficients *A(ij)* and *B(ij)*, the cooling-fluid and the air outlet temperatures are calculated following equations (14) and (17). At the end of the computation in cell *ij*, the output temperature is set as the inlet temperature of cell *i+1,j*. The outlet temperature of column *j* is that of cell *nj*.

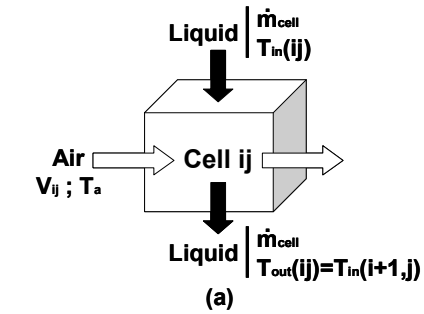

Figure 5: (a) Thermal balance at cell ij (b) loop of column j outlet temperature computation.

To calculate the outlet temperature of the entire heat exchanger, the computation procedure shown in Figure 4b is repeated for all the *m* columns. Finally, the outlet temperature of the heat exchanger is the average temperature of the various columns output:

$$T_{out} = \frac{\sum_{j=1}^{m} T_{out}(nj)}{m} \quad (17)$$

The heat evacuated by the heat exchanger is given by the following expression:

$$P = \dot{m}.C_p.(T_{in} - T_{out}) \quad (18)$$

Aerodynamic computation

When the outdoor cold air passes through a heat exchanger cell, it is heated and its density changes. We use a linear extrapolation of the tables in Kays and Crawford [30] to calculate this variation. Knowing the air density downstream of the heat exchanger, the air velocity can be calculated by considering mass conservation:

$$\rho_{air,upstream}.V_{air,upstream} = \rho_{air,downtsream}.V_{air,downstream} \quad (19)$$

Measurements carried out on a Valeo radiator have determined typical pressure loss variations as a function of the air velocity and for different fluid flow rates (Figure 6).

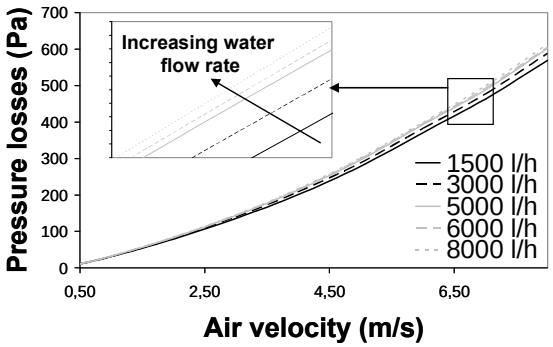

Figure 6: Air pressure losses through a Valeo heat exchanger as a function of air velocity for different water flow rates.

It can be noticed that for cooling-fluid flow rates greater than 8000 l/h, pressure loss coefficients become independent of the cooling-fluid flow rate; also, for air velocities lower than 2 m/s, pressure loss coefficients become independent of the cooling-fluid flow rate. For cooling-fluid flow rate below 8000 l/h and an air velocity above 2 m/s, the pressure-drop – air-velocity curves vary slightly between different cooling-fluid flow rates and follow (for a given cooling-fluid flow rate) a power law of the form:

$$PL = u.V^{v} \quad (20)$$

For a given air velocity, it can be observed that the pressure losses follow a polynomial function of the cooling-fluid flow rate. Thus, for a given cooling-fluid flow rate between the corresponding experimental curves, polynomial interpolation permits calculation of the pressure losses corresponding to the different air speeds. With the pressure loss coefficients values calculated for different air velocities (values at the nodes), the power law of equation (20) can then be deduced.

RESULTS AND ANALYSIS

This section focuses on analyzing the effects of upstream air flow nonuniformity on heat exchanger performance, and the effects of heat exchanger positioning in the cooling system. Then, a new control approach based on the optimized results is proposed.

Effects of air flow nonuniformity

In this section a heat exchanger matrix of 4×4 cells is considered. Computations are performed, using the two-dimensional code described above, for an overall cooling-fluid flow rate 6000 l/h, inlet temperature 90 °C, and incoming air temperature 20 °C. This section aims at determining how heat exchanger performance varies as a function of the rms σ that characterizes the uniformity of the upstream velocity distribution.

Figure 7 shows outlet water temperature and thermal power evacuated by the 4×4 cell heat exchanger as a function of the relative rms σ / V_m for different upstream mean velocities.

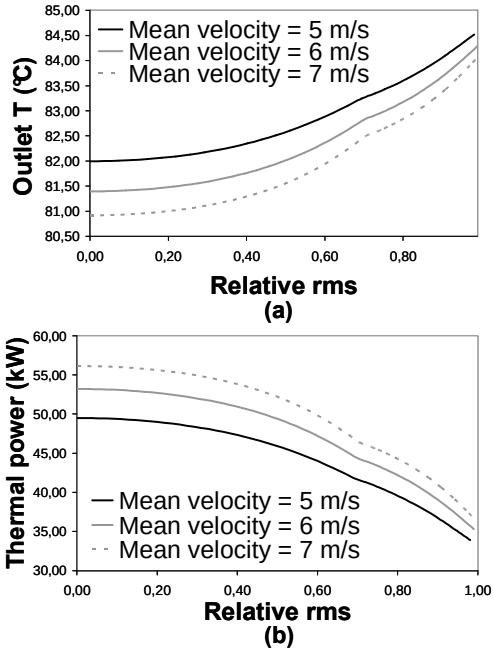

Figure 7: Variations in (a) cooling-fluid outlet temperature and (b) thermal power of heat exchanger as a function of relative rms for different mean air velocities.

It is observed that the nonuniformity in the upstream velocity distribution increases the cooling-fluid outlet temperature of the heat exchanger. For example, for mean velocity 7 m/s (i.e. for the same airflow rate passing through the heat exchanger), increasing the relative rms from 0 to 1 increases the outlet temperature from 80.9 °C to 84.1 °C. The heat exchanger thermal power (Figure 7b) decreases from 56.2 kW to 36.4 kW when the relative rms increases from 0 to 1, a 35% decrease compared to a uniform upstream velocity distribution. It is noted that only 7% of this 35% power decrease occurs for σ varying from 0 to $0.5V_m$. Therefore, heat exchangers surfaces should be placed in the underhood compartment where the air velocity distribution is most uniform.

A more remarkable feature of the nonuniformity effects is the influence of permutations between air velocities on the different heat exchanger cells, even for fixed mean air velocity and fixed standard deviation. Figure 8 shows the cooling-fluid outlet temperature and the thermal power evacuated by a 4×4

cell heat exchanger as a function of the relative rms σ / V_m for the two permutation configurations of Figure 9; the mean air velocity is 7 m/s.

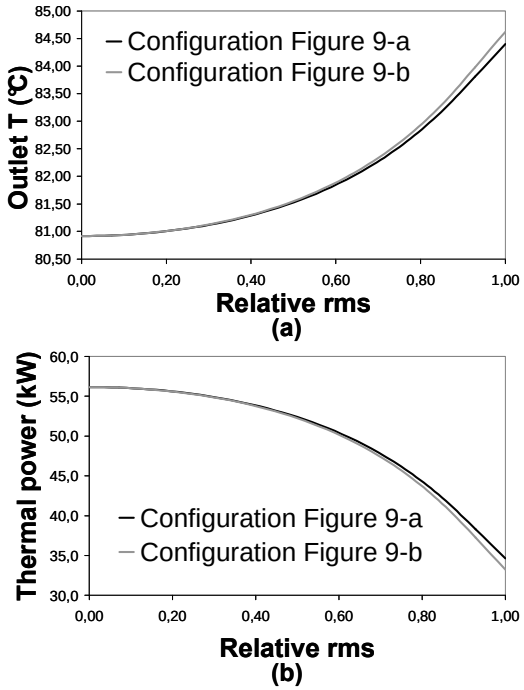

Figure 8: Variations in (a) cooling-fluid outlet temperature and (b) thermal power of the heat exchanger as a function of relative rms for different velocity permutation configurations at mean air velocity 7 m/s.

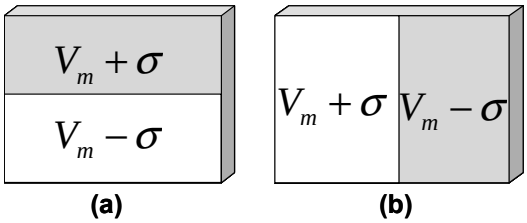

Figure 9: Two velocity permutation configurations for a heat exchanger.

It is noted that the thermal power evacuated (the cooling-fluid outlet temperature) in the configuration of Figure 9a is greater (lower) than that in the configuration of Figure 9b. In other terms, for a fixed mean and standard deviation of the upstream air velocity distribution, a heat exchanger cooled by $V_m + \sigma$ air flow on its top part and $V_m - \sigma$ air flow on its bottom part evacuates more heat than when it is cooled by $V_m + \sigma$ air flow on its right part and $V_m - \sigma$ air flow on its left part. For an order of magnitude estimate: note that for a mean air velocity of 7 m/s, varying the relative rms from 0 to 1 changes the thermal power evacuated by the heat exchanger in the configuration of Figure 9a from 56.2 kW to 34.6 kW as against 56.2 kW to 33.2 kW in the configuration of Figure 9-b. It is also noted that the difference between the two curves in Figure 8 starts to be significant at a relative standard deviation of almost 0.5. Therefore, attention should be paid to the air inlet *high* and *low* velocity positioning with respect to the heat exchanger surface, especially at high rms. In this sense it is preferable (as shown above), for example, to superpose high-velocity regions of the air inlet on the top parts of the heat exchanger, and low-velocity regions of the inlet air on the bottom parts of the heat exchanger, than to superpose respectively high and low air-inlet velocity regions on the left and right heat-exchanger parts.

Effects of heat exchanger positioning

Let us imagine a different positioning for heat exchangers in the cooling system from that presented in the introduction: heat exchangers are placed in the same plane Y vis-à-vis the airflow (Figure 10). We call this configuration "in plane".

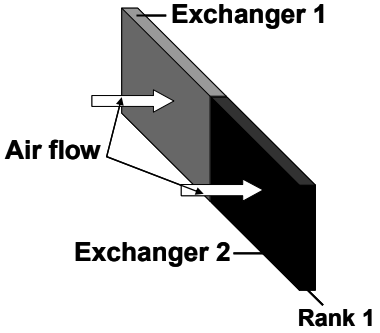

Figure 10: Two heat exchangers in in-plane configuration.

For the in-plane configuration, the transverse space Y necessary for heat exchanger implementation is larger, but the longitudinal extension (in X) is reduced. Thus, the in-plane configuration seems *a priori* more advantageous from an aerothermal point of view but more constraining on the underhood implementation than the in-rank arrangement.

To evaluate the aerothermal effect of relative heat exchanger positioning, computations (with the 2D code described in section 4) of the heat exchanger power, pressure loss and downstream air temperature were carried out on a simplified vehicle cooling system composed only of two heat exchangers and a fan. Heat exchangers are taken as 4×4 cell matrices. In this study we use the upstream air velocity field induced in a wind tunnel on the air intakes of a real vehicle (Peugeot 207) and measures by LDV. From these measurements, the velocity field is discretized into 32 cells as shown in Figure 11.

V_m	$0.75V_m$	$0.75V_m$	$0.75V_m$	$0.75V_m$	$0.75V_m$	$0.75V_m$	V_m
$0.75V_m$	V_m	V_m	V_m	V_m	V_m	V_m	$0.75V_m$
$0.75V_m$	V_m	V_m	V_m	V_m	V_m	V_m	$0.75V_m$
$0.75V_m$	V_m	V_m	V_m	V_m	V_m	V_m	$0.75V_m$

Figure 11: Approximate representation of real air velocity distribution on front end openings of real vehicle in driving situation.

Heat exchangers are positioned in nine configurations with respect to the airflow, as shown in Figure 12.

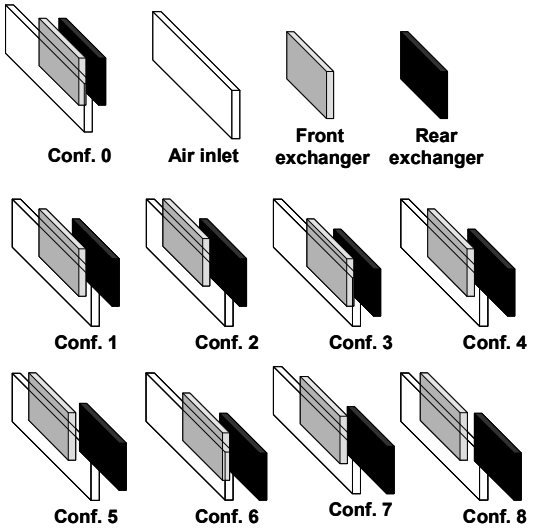

Figure 12: Different configurations of the two exchanger arrangements; in gray, the front heat exchanger, in black, the rear heat exchanger. The transparent frame represents the mesh of the upstream air velocity field.

The cooling-fluid flowing through the two exchangers is taken as water at inlet temperature 95 °C. The water flow rate in each cell is set at 1500 l / h (recall that water enters through the top of the heat exchanger and is distributed among the different columns before leaving from the bottom). The air temperature is taken as 20 °C. Results obtained for configurations 1 to 8 are compared to configuration 0, which corresponds to the in-rank reference arrangement found in most vehicles: the two heat exchangers are placed one behind the other. For this comparison, the relative difference called "deviation percentage" is calculated for each case:

$$E_r = \frac{Value(.Tested.Config) - Value("in\ rank")}{Value("in\ rank")}.100 \quad (21)$$

Table 1 summarizes the value of E_r obtained for the different configurations.

It should be noticed that percentages of thermal power improvements in Table 1 are relative to the overall thermal power of the system, which is the sum of that of the two heat exchangers. In other words, if one focuses only on the thermal power of the downstream heat exchanger, the power improvement percentages in Table 1 should be multiplied by 2.

Configuration	**1**	**2**	**3**	**4**
Heat exchangers thermal power	1.12	2.20	1.12	2.23
Pressure Losses	-0.06	-0.45	-0.06	-0.12
Downstream mean air temperature	-0.004	-0.009	-0.004	-0.009

Configuration	**5**	**6**	**7**	**8**
Heat exchangers thermal power	3.32	2.2	3.32	4.4
Pressure Losses	-0.52	-0.45	-0.52	-0.91
Downstream mean air temperature	-0.013	-0.008	-0.012	-0.017

Table 1: Deviation percentages with respect to the reference in-rank configuration.

It is noted that configuration 8 is the most optimized. This is in fact an in-plane configuration (configurations 1 to 7 are intermediate cases between the in-rank and in-plane arrangements). The in-plane configuration is better than the in-rank configuration (0) and the other intermediate configurations (1–7) in terms of thermal power, pressure loss and air temperature downstream of the cooling system. Compared to the in-rank configuration, the in-plane configuration presents:
- 4.4% increase in thermal power
- 0.9% decrease in pressure losses
- 0.02%.decrease in air temperature downstream of the heat exchangers

Consider now the two cases shown in Figure 13.

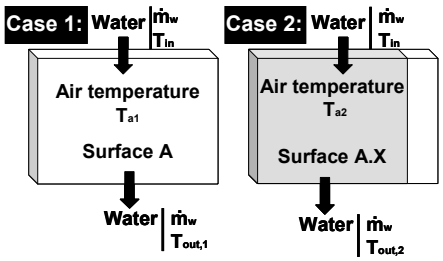

Figure 13: Two heat-exchanger configurations: front faces subject to different air temperatures.

In Figure 13, the heat exchanger in gray (case 2) has smaller frontal area than that of the first case: its surface is equal to X times (X<1) that of the first case.

For the same water flow rate and air velocity crossing the two heat exchangers, one can write:

$$T_{out,1} = \frac{C-Q}{C+Q}.T_{in} + \frac{2Q}{C+Q}.T_{a1} \quad (22)$$

$$T_{out,2} = \frac{C-Q.X}{C+Q.X}.T_{in} + \frac{2Q.X}{C+Q.X}.T_{a2} \quad (23)$$

where:

$$C = 2.\dot{m}.C_p \quad (24)$$

$$Q = h(\dot{m};V).S \quad (25)$$

Therefore, in order that the second heat exchanger evacuates the same amount of heat as the first, the fraction X should be:

$$X = \frac{2Q.C.T_{in} + 2Q^2.T_{a1} - 2Q.C.T_{a2} - 2Q^2.T_{a2}}{2C.Q.T_{in} - 2Q.C.T_{a1}} \quad (26)$$

Figure 14 shows the variation in X as a function of air temperature cooling the second heat exchanger, based on equation (26). The computation is performed for water flow rate 6000 l/h, air velocity 7 m/s and water inlet temperature 90 °C.

For the same air flow rate through the two heat exchangers, the greater the air temperature 1 upstream of the first heat exchanger, the smaller the surface fraction required for the second heat exchanger to evacuate the same heat as that evacuated by facing cooler air. Note that the air temperature 1 is always greater than the air temperature 2.

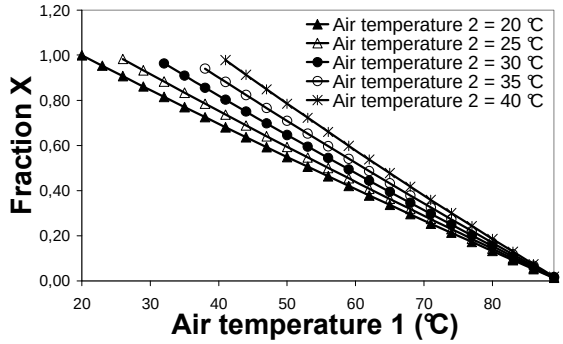

Figure 14: Variation in the heat exchanger surface fraction X as a function of air temperature 1, for different air temperatures 2 (equation (26)).

For an air temperature 2 of 20°C, for example, the following cases can be noted:

- X = 0.7 for an air temperature 1 of 40°C,
- X = 0.5 for an air temperature 1 of 53.4°C

Thus, a heat exchanger of a given frontal surface, placed directly in an air flow at 20 °C evacuates the same amount of heat as a heat exchanger of double the surface area placed downstream of another heat exchanger that heats the air up to 53.4°C.

Control procedure

This section discusses a new monitoring tool that can be used to optimize underhood aerothermal management. This tool lets one adapt heat exchanger performances to engine cooling requirements and increase the heat exchanger heat-extraction power in critical situations such as the vehicle slowdown phase or the thermal soak phase (vehicle stops after a significant heating load).

On the basis of the optimization results above on the superposition of two heat exchangers in a vehicle cooling system, the principle of the control approach is to separate in the Y direction (the vehicle width) the vehicle condenser (heat exchanger at rank 1 in the above analysis) from the radiator (heat exchanger 2) in order to increase the heat extraction by the radiator in critical situations where the engine overheats. This control is managed by a thermocouple placed in the cooling water upstream from the radiator inlet (the engine exit). Depending on the radiator inlet temperature, in a given thermal driving situation, the power requirements of the radiator and the need to increase power over the normal situation are identified and the condenser is then moved to a distance that corresponds to the desired increase in power. For example, say that in a given situation the thermocouple placed at the radiator inlet indicates a need to increase the radiator power by 6% over its normal value. In this case, the control process moves the condenser in the Y direction with respect to the radiator so that they will be in configuration 7 (Table 1) in Figure 12.

In order to give a simple schematic diagram of this control application, consider a simplified vehicle cooling system consisting only of one condenser and one radiator (as in a Peugeot 207 without turbocompressor). In other vehicle types, the same principles are applicable to other heat exchanger types (such as a charged air cooler or engine oil cooler). The technical principle of the proposed control procedure is described in Figure 15a.

The thermocouple at the radiator inlet sends the instantaneous temperature value to the automatic control system (step 1 in the procedure diagram, Figure 15). This, in turn, verifies in real time if the temperature reaches the critical value T_i. On the other hand, the control system contains a correspondence law between the critical temperatures T_i and positions Y_i between heat exchanger i (radiator) and the other heat exchangers. If one of the critical temperatures T_i is reached, the control

system automatically tells exchanger *i* to move by a distance Y_i from the other heat exchangers corresponding to the values previously recorded. The control system also controls the elongation of the pipe to the same distance Y_i (both commands described correspond to number 2 in the procedure diagram). Figure 15b shows the cooling system of Figure 15a (reference configuration) once the control procedure is applied.

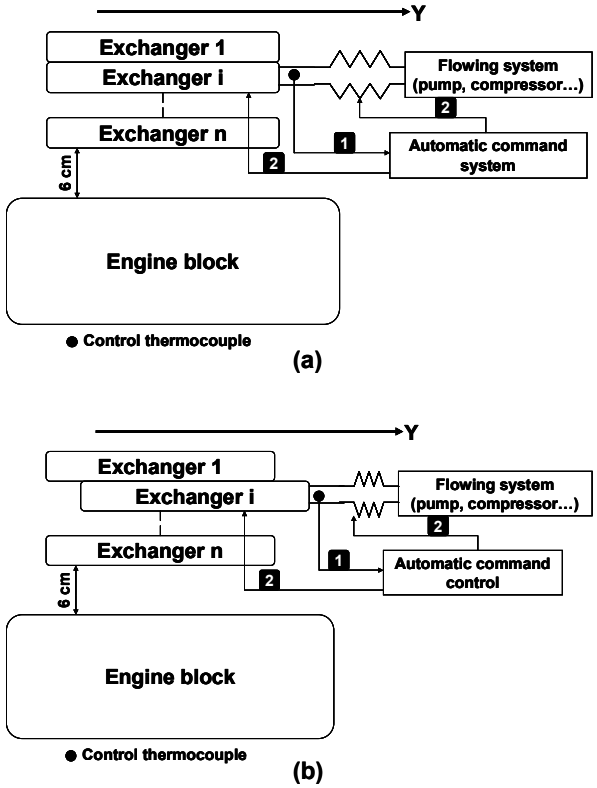

Figure 15: (a) Control procedure for heat exchanger i displacement; (b) systems after control procedure is applied.

It should be noted that in the version of the control procedure here, the control can affect the displacement of one or more heat exchangers in the cooling system. Therefore, Figure 15a shows the command principle (control) for displacement of a given heat exchanger *i* with respect to others in the same system. The full procedure (even in a cooling system containing other heat exchangers in addition to the radiator and condenser) consists in the superposition of the basic procedures such as those described in Figure 15a.

The economic attraction of this control procedure is evident from its use in normal, noncritical engine operation. In normal vehicle operation, this control procedure can increase the heat extraction capacity of the cooling system for the same work of the water pump and the air-conditioning system compressor. Thus, one could achieve the same heat-extraction capacity by the heat exchangers for smaller pump and compressor work, which reduces vehicle fuel consumption (since the work of the pump and compressor correspond to losses in engine power).

CONCLUSIONS

Several studies [22-26] on louvered-fin heat exchangers for underhood applications have shown that the thermal performance of these heat exchangers is strongly dependent on the geometric parameters of the heat exchanger (e.g. distance between fins, tube height, and fin angle) and the operating conditions of the two fluids, air and water (their mass flow rates and inlet temperatures). However, few studies have focused on how to control these parameters to enhance the heat exchanger's heat-extraction capacity. Most underhood thermal management work has concentrated on underhood thermal management by temperature and heat flux measurements [31-34] with fixed heat exchangers. In the present work, the numerical investigation is dedicated to optimization of the heat exchanger thermal power by acting on the dynamical positioning of the heat exchanger in the underhood. This analysis also shows explicitly how to affect the different parameters that impact the heat exchanger performance in order to optimize its functioning.

It has been shown that an increase in the nonuniformity (represented by σ) of the upstream velocity distribution increases the heat-exchanger water outlet temperature and thus decreases its thermal power. As an example, it was observed that increasing σ from 0 to V_m decreased the heat-exchanger thermal power by 35% with respect to a uniform V_m airflow; the decrease between 0 and $0.5V_m$ was only 7%.

On the other hand, compared to the reference in-rank configuration of the heat exchangers in which the different heat exchangers are positioned one behind the other) the in-plane configuration in which the different heat exchanger surfaces are in the same *x* coordinate vis-à-vis the air flow showed an increase of overall thermal extraction power of 4.4% (8.8 % for the downstream exchanger) and a decrease in the pressure losses of 0.9%.

Finally, a new monitoring procedure that can be used for optimizing the underhood aerothermal management is proposed based on the numerical findings. This procedure permits adaptation of heat-exchanger performance to the engine cooling requirements and increasing the heat exchangers' heat- extraction power in critical situations, as in the slowdown phase or the thermal soak phase of a vehicle (vehicle stops after a significant heating load).

REFERENCES

[1] G. Xie, B. Sunden, Q. Wang, and L. Tang, Performance predictions of laminar and turbulent heat transfer and fluid flow of heat exchangers having large tube-diameter and large tube-row by artificial neural networks, Int.J. Heat Mass Transfer 52 (2009) 2484-2497.

[2] M.I. Hasan, A.A. Rageb, M. Yaghoubi, and H. Homayoni, influence of channel geometry on the performance of a counter flow microchannel heat exchanger, Int.J. Thermal Sciences (2009).

[3] M.R. Salimpour, Heat transfer coefficients of shell and coiled tube heat exchangers, Experimental Thermal and Fluid Science 33 (2009) 203-207.

[4] R. Toé, A. Ajakh, and H. Peerhossaini, Heat transfer enhancement by Gortler instability, Int. J. Heat Fluid Flow, 23 (2002) 194-204.

[5] P. Zhang, P.S. Hrnjak, Air-side performance evaluation of three types of heat exchangers in dry, wet and periodic frosting conditions, International Journal of Refrigeration (2009).

[6] A. Ajakh, Kestoras M.D, R. Toé, and H. Peerhossaini, Influence of forced perturbations in the stagnation region on Gortler instability, AIAA Journal, 37 (1999) 1572-1577.

[7] H. Peerhossaini, and F. Bahri, On the spectral distribution of the modes in nonlinear Gortler instability, Thermal and Fluid Science, 16 (1998) 195-208
.

[8] C. Habchi, T. Lemenand, D. Della Valle, H. Peerhossaini, Liquid-liquid dispersion in a chaotic advection flow, International Journal of Multiphase Flow 35 (2009) 485-497.

[9] C. Habchi, S. Ouarets, T. Lemenand, D. Della Valle, J. Bellettre, H. Peerhossaini, Influence of viscosity ratio on droplets formation in a chaotic advection flow, International Journal of Chemical Reactor Engineering 7 (2009) A50.

[10] Y. Lai, N. Cordero, F. Barthel, F. Tebbe, J. Kuhn, R. Apfelbeck and D. Wurtenberger, Liquid cooling of bright LEDs for automotive applications, Applied Thermal Engineering 29 (2009) 1239-1244.

[11] M.J. Lawson and K.A. Thole, Heat transfer augmentation along the tube wall of a louvered fin heat exchanger using practical delta winglets, Int.J. Heat Mass Transfer 51 (2008) 2346-2360.

[12] S. Ferouillat, P.Tochon, C. Garnier and H. Peerhossaini, Intensification of heat-transfer and mixing in multifunctional heat exchangers by artificially generated streamwise vorticity, Applied Thermal Engineering, 26 (2006) 1820-1829.

[13] S. Ferouillat, P.Tochon and H. Peerhossaini, Open-loop thermal control of exothermal chemical reactions in multifunctional heat exchangers, Int.J. Heat Mass Transfer 26 (2006) 2479-2490.

[14] A.R. Doodman, M. Fesanghray, and R. Hosseini, A robust stochastic approach for design optimization of air cooled heat exchangers, Applied Energy 86 (2009) 1240-1245.

[15] J. Guo, M. Xu, and L. Cheng, The application of field synergy number in shell-and-tube heat exchanger optimization design, Applied Energy 86 (2009) 2079-2087.

[16] S. Ferrouillat, P. Tochon, H. Peerhossaini, Micromixing enhancement by turbulence: application to multifunctional heat exchangers, Chemical Engineering and Processing 45 (2006) 633-640.

[17] A.K. Gholap and J.A. Khan, Design and multi-objective optimisation of heat exchangers for refrigerators, Applied Energy 84 (2007) 1226-1239.

[18] R.Hilbert, G. Janiga, R. Baron and D. Thévenin, Multi-objective shape optimization of a heat exchanger using parallel genetic algorithms, International Journal of Heat and Mass Transfer 49 (2006) 2567-2577.

[19] K. Foli, T. Okabe, M. Olhofer, Y. Jin and B. Sendhoff, Optimization of micro heat exchanger: CFD, analytical approach and multi-objective evolutionary algorithms, International Journal of Heat and Mass Transfer 49 (2006) 1090-1099.

[20] C. Habchi, T. Lemenand, D. Della Valle, H. Peerhossaini, Alternating mixing tabs in multifunctional heat exchanger-reactor, Chemical Engineering and Processing, doi:10.1016/j.cep.2009.07.003

[21] M. Khaled, F. Harambat and H. Peerhossaini, Effects of upstream air flow statistics on air-cooled heat exchanger performance: analytical and empirical determination of thermal power, International Journal of Heat and Mass Transfer, submitted 2010.

[22] C. Oliet, A. Oliva, J. Castro, and C.D. Pérez-Segarra, Parametric studies on automotive radiators, Applied Thermal Engineering 27 (2007) 2033-2043.

[23] Z.G.. Qi, J.P. Chen, and Z.J. Chen, Parametric study on the performance of a heat exchanger with corrugated louvered fins, Applied Thermal Engineering 27 (2007) 539-544.

[24] A. Witry, M.H. Al-Hajeri, and A.A. Bondok, Thermal performance of automotive aluminium plate radiator, Applied Thermal Engineering 25 (2005) 1207-1218.

[25] E. Carluccio, G. Starace, A. Ficarella, and D. Laforgia, Numerical analysis of a cross-flow compact heat exchanger for vehicle applications, Applied Thermal Engineering 25 (2005) 1995-2013.

[26] A. Lozano, F. Barreras, N. Fueyo and S. Santodomingo, The floor in an oil/water heat exchanger for the automotive industry, Applied Thermal Engineering 28 (2008) 1109-1117.

[27] A. Jerhamre and A. Jonson, Development and validation of coolant temperature and cooling air flow CFD simulations at Volvo cars, SAE technical paper 2004-01-0051.

[28] A. Waschle, Numerical methods, 3-dimensional, Progress in Vehicle Aerodynamics II Thermo-Management, 2002.

[29] A. Waschle, Numerische Simulation der Stromung durch einen Pkw-Kuhler und Berechnung der Warmeubertragung, Diplomarbeit bei der DaimlerChrysler AG, 2000.

[30] W.M. Kays and M.E. Crawford, Convective Heat and Mass Transfer, McGraw–Hill, New York, 1993.

[31] M. Khaled, F. Harambat and H. Peerhossaini, A quantitative method for assessment of car inclination effects on thermal management of the underhood compartment, Journal of Thermal Science and Engineering Applications – Transaction of ASME, March 2009, Vol. 1/014501-5.

[32] M. Khaled, F. Harambat and H. Peerhossaini, Temperature and heat flux behavior of complex flows in car underhood compartment, Heat Transfer Engineering, in press.

[33] M. Khaled, F. Harambat and H. Peerhossaini, Underhood thermal management: temperature and heat flux measurements and physical analysis, Applied Thermal Engineering, in press.

[34] M. Khaled, B. Garnier, F. Harambat and H. Peerhossaini, A new method for simultaneous measurement of convective and radiative heat flux in car underhood applications, Measurement Science and Technology, in press.